Influence of phenyl-attached substituents on the vibrational and electronic spectra of meso-tetraphenylporphyrin: A DFT study

ARTICLE *in* COMPUTATIONAL AND THEORETICAL CHEMISTRY · MARCH 2015

Impact Factor: 1.55 · DOI: 10.1016/j.comptc.2015.03.009

6 AUTHORS, INCLUDING:

Chanisorn Ngaojampa

Chiang Mai University

5 PUBLICATIONS **13** CITATIONS

SEE PROFILE

Supawadee Namuangruk

National Nanotechnology Center, Thailand

72 PUBLICATIONS **717** CITATIONS

SEE PROFILE

Vinich Promarak

Vidyasirimedhi Institute of Science and Tec…

97 PUBLICATIONS **1,416** CITATIONS

SEE PROFILE

Nawee Kungwan

Chiang Mai University

54 PUBLICATIONS **217** CITATIONS

SEE PROFILE

Computational and Theoretical Chemistry 1062 (2015) 1–10

Contents lists available at ScienceDirect

Computational and Theoretical Chemistry

journal homepage: www.elsevier.com/locate/comptc

Influence of phenyl-attached substituents on the vibrational and electronic spectra of meso-tetraphenylporphyrin: A DFT study

Chanisorn Ngaojampa [a], Supawadee Namuangruk [b], Yaowarat Surakhot [c], Vinich Promarak [d], Siriporn Jungsuttiwong [c], Nawee Kungwan [a,*]

[a] Department of Chemistry, Faculty of Science, Chiang Mai University, Chiang Mai 50200, Thailand
[b] National Nanotechnology Center, National Science and Technology Development Agency, Klong Luang, Pathumthani 12120, Thailand
[c] Center for Organic Electronic and Alternative Energy, Department of Chemistry and Center of Excellence for Innovation in Chemistry, Faculty of Science, Ubon Ratchathani University, Ubon Ratchathani 34190, Thailand
[d] School of Chemistry, Institute of Science, Suranaree University of Technology, Nakhon Ratchasima 30000, Thailand

ARTICLE INFO

Article history:
Received 23 January 2015
Received in revised form 25 February 2015
Accepted 10 March 2015
Available online 30 March 2015

Keywords:
Porphyrin
Dye-sensitized solar cells (DSSCs)
DFT
TD-DFT

ABSTRACT

The effects of substituents attached to phenyl groups of free base meso-tetraphenylporphyrin (H_2TPP) on its geometrical structure, vibrational spectra and electronic spectra of H_2TPP derivatives namely **FB1-8** are predicted by the density functional theory (DFT) and time-dependent DFT (TD-DFT) calculations. The calculations revealed no notable changes in the geometrical structures of the substituent-altered H_2TPP derivatives. Changes in the vibrational modes are mainly observed in the phenyl moieties of the porphyrin molecules, and less significant in the central porphine ring except for two derivatives, **FB4** and **FB8**. The substituent effects have more influence on the electronic structures of the studied porphyrins. The introduction of strong electron-donating and – withdrawing substituents, i.e. dimethylamino and nitro groups in this study, to the four phenyl rings results in the splits in the Soret or B band of the derivatives due to a major rearrangement in energy levels of the molecular orbitals. The dimethylamino groups (in **FB4**) dramatically increase the Q band intensities of the molecule. The intensified Q bands are the results of strong charge-transfer from the substituents to the porphine core upon the electronic excitations. Among the eight designed dyes, **FB4** is promising to be further developed as metalloporphyrin-based dye. The understandings of the electronic structure and optical properties according to the molecular modifications are useful in the rational design of the zinc-porphyrin-based sensitizer in the solar cells.

1. Introduction

Porphyrin has been long known for its fascinating photochemical property that drives the photosynthesis in plants and bacteria. This has inspired many studies in the pursuits of its applications, such as nonlinear optical materials [1,2], photodynamic therapy [3,4], nanosensors [5,6] and photovoltaic devices. The last has been gaining more and more spotlight in recent years after the early-2000s breakthrough of dye-sensitized solar cells (DSSCs) [7–14], a decade after Grätzel's group proposed a novel architecture of sunlight harvesting panels consisting of a sensitizing ruthenium-based dye and the semiconductor electrode [15].

Projected to replace the rare and environment-irritating ruthenium dyes, the chlorophyll-inspired sensitizers based on porphyrin dyes premiered in 2007 when Campbell et al. [8] tested the photovoltaic performances of a series of zinc-porphyrin dyes. The light-to-electricity power conversion efficiencies (η) of the dyes were reported in the range of 5–8%. In less than a decade, porphyrin-based sensitizers have been impressively improved in their performances [10]. The co-sensitizing of **YD2-*o*-C8** zinc-porphyrin derivatives and **Y123** dye in cobalt electrolyte with $\eta = 12.3\%$ marks the first time a porphyrin-based sensitizer edged out ruthenium dyes in efficiency (10–11%) [10,14]. In less than three years, a stronger candidate porphyrin dye, coded as **SM315**, was reported by Grätzel's group having $\eta = 13\%$ marking the most-efficient porphyrin-based sensitizers reported so far [16]. The back-to-back success also suggests the potential of further development of porphyrin derivatives as light-collecting antennae.

Spectroscopic studies of dye molecules are considered to be fundamental for the design and screening of the sensitizers. Spectra of porphyrin had attracted scientists' interest prior to the birth of porphyrin-based DSSCs. One of the early landmark works was Gouterman's four-orbital model, which successfully explained

* Corresponding author. Tel.: +66 53 943341x101; fax: +66 53 892277.
E-mail address: naweekung@gmail.com (N. Kungwan).

http://dx.doi.org/10.1016/j.comptc.2015.03.009
2210-271X/

the origin of the visible Q bands and the intense ultraviolet/near-ultraviolet B bands (also known as Soret bands) based on the π–π* excitations involving four central orbitals: two highest occupied and two degenerated lowest unoccupied orbitals [17]. In the quest of DSSC development, the dyes are greatly preferred to absorb a wide spectrum of light especially in the reddish visible region, the usual location for Q bands, which generally gives higher incident monochromatic photon-to-current efficiency (IPCE) [15,18–20]. Absorbance enhancement of porphyrin dyes can be approached by the introduction of electron-donating/-withdrawing substituents to the porphyrin core, especially extensions at meso-carbons which generally results in more intense and more red-shifted Q and B bands compared to those at pyrrolic β-carbons [11,14,21]. Moreover, bulky meso-substitutions also reduce the π-stacking interaction which causes aggregation of sensitizers [22]. Besides the positions of modification, the substituent groups themselves also contribute to the enhancement of dye sensitizers. Electron-donating groups were reported to promote the push–pull mobilization of excited electron and thus the device efficiency [23–25]. Such push–pull electronic architecture is also featured in the best-to-date porphyrin dyes, **SM315**, mentioned earlier.

In this report, we move our focus to the effect of substituents from more distant locations, i.e. from the parts that are not directly attached to porphyrin cores. This is expected to be helpful to the fine-adjustment of the light-harvesting capacity of sensitizing dyes. The core molecule of study is H_2TPP of which zinc complex (ZnTPP) has been used as the template for several high-efficiency porphyrin-based dyes to date (for example **Zn-1a**, **Zn-3**, **GD2**, **2b-bd-Zn**, **YD2**, **YD2-*o*-C8** and the highly efficient **SM315** [7,8,11–14]). To investigate the effect systematically, the influence of common electron-affecting substituents, i.e. methyl, hydroxyl, dimethylamino, methyl carboxyl, cyano and nitro groups, on the four meso-phenyl rings were speculated relying on their vibrational and electronic spectra calculated by density functional theory (DFT) [26] and time-dependent DFT (TDDFT) [27], the methods which had made a number of successful predictions in earlier theoretical studies of dye sensitizers [8,28–30].

2. Computational procedures

Structures of H_2TPP and its seven derivatives, numbered as **FB1** to **FB8** (Fig. 1), are modeled and optimized using Kohn–Sham DFT at B3LYP/6-31G(d) [31,32] level without any symmetry constraints. The vertical excitation energies of the 50 lowest spin-allowed singlet transitions were calculated using TD-DFT on B3LYP hybrid functional. Solvent effect from dichloromethane (CH_2Cl_2) was also taken into account by the non-equilibrium model of the conductor polarized continuum model (C-PCM) framework [33,34]. The contribution of molecular orbitals in the electronic transition was calculated using the GaussSum program version 3.0 [35]. All calculations were carried out using Gaussian09 software package [36]. The vibrational and electronic spectra were visualized using Gabedit program [37].

3. Results and discussions

3.1. Ground-state geometry

The optimized structures of H_2TPP and its meso-substituted derivatives (Fig. 2) settle in a square-planar geometry with minor distortions (no more than 5° of torsional deviations from 0° or 180°). The calculated common structural parameters of **FB1-8** (i.e. the porphine cores and some parts of phenyl rings) are listed in Supplementary Information. From this part of the result, it can be commented that the overall structures of the porphine centers remain undisturbed as the substituents are introduced to the phenyl rings. Only **FB4** could be closest to being "disturbed" as it shows the largest deviation in C_β–C_β–C_α–C_m and N–C_α–C_m–C_1 dihedral angles. However, the degree of deviation is still minimal. Its C_m–C_1 bond length also shrinks 0.003 Å compared to other derivatives in this series. These suggest a slight plane distortion and ring contraction of **FB4**.

The π-conjugation systems of the porphine centers and phenyl wings are disconnected as the phenyl rings make angles of about 70° to the porphine centers (represented by C_α–C_m–C_1–C_2 dihedral angles). Again, **FB4** stands out of other derivatives as its porphine-phenyl interplanar angles lie at 64.8°, while others have this angle in the range of 68–70°.

3.2. Vibrational spectra

The central porphine skeleton can be categorized as a planar molecule of D_{2h} symmetry. Mode symbols for porphine used in this study follow Li and Zgierski's mode numbering [38]. Detailed

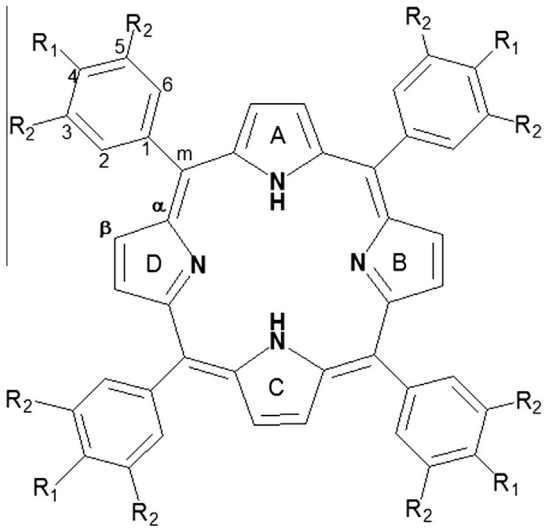

Free-base porphyrins	R1	R2
FB1	H	H
FB2	Me	H
FB3	OH	H
FB4	NMe2	H
FB5	COOMe	H
FB6	CN	H
FB7	NO2	H
FB8	H	Me

Fig. 1. Eight compounds of the study along with their code names and atomic numberings. The ring names (A, B, C and D) are according to IUPAC nomenclature [40].

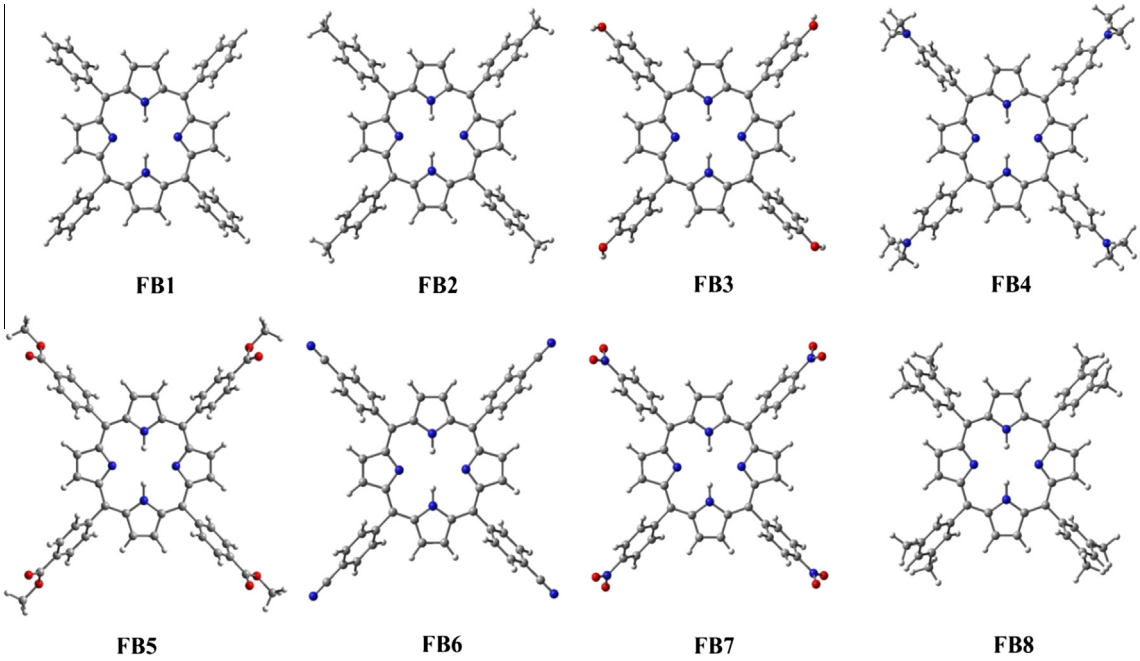

Fig. 2. Optimized geometries of free-base porphyrins by B3LYP/6-31G(d) level of theory.

discussions of local modes of meso-phenyl rings are omitted as they are considered trivial. The B3LYP-predicted vibrational spectra of the H_2TPP derivatives are presented in Supplementary Information. The spectrum assignments for the vibrational modes are given in Tables 1 and 2.

3.2.1. Raman spectra

Raman spectra reveal a number of observable changes in porphine ring vibration modes in substituent-altered H_2TPP. In general, the magnitude of substituent effects on phenyl ring are relatively smaller compared to the effects caused by direct substitution on C_m of the central porphine rings as studied by Zhang et al. [39]. The observable changes of vibrational modes in porphine ring include.

3.2.1.1. ν_1 mode. This mode mainly represents meso-phenyl bond (C_m–C_1) symmetric stretching. For this mode, all substituents give minor upshifts (by the extent of 1–3 cm^{-1}) from the original ν_1 frequency of H_2TPP at 1260 cm^{-1}, except **FB4** and **FB8**, which give larger leap to 1273 and 1329 cm^{-1} respectively.

3.2.1.2. ν_6 and ν_{15} modes. The in-phase pyrrole ring breathing (ν_6) remains unchanged at 988 cm^{-1} for the whole series of para substituted derivatives of H_2TPP (**FB1**-7). However, the band loses its intensity when para substituents are introduced to the phenyl rings (**FB2**-7). Again, **FB8** is a special case for expressing ν_6 band at 1002 cm^{-1}. Meanwhile, the out-of-phase pyrrole ring breathing (ν_{15}) expresses no substituent-sensitivity as the band stays bound at 1028 ± 1 cm^{-1} for the whole series of H_2TPP derivatives.

Table 1
Band positions and assignment of calculated Raman bands of **FB1**-**8**.

Band positions (cm^{-1})								Mode number	Assignment
FB1	**FB2**	**FB3**	**FB4**	**FB5**	**FB6**	**FB7**	**FB8**		
169	169	170	172	169	172	171	170	ν_{18} (A_g)*	ν(pyr trans) o.o.ph.**
339	334	334	326	321	330	325	340	ν_8 (A_g)	ν(pyr trans) i.ph.**
418	420	423	427	420	414	423	226		Phenyl
636	653	657	652	652	654	648	522		Phenyl
863	860	857	846	865	860	857	833		Phenyl
899	902	903	901	902	902	906	954	ν_7 (A_g)	ν(pyr def) sym
988	988	988	988	988	988	988	1002	ν_6 (A_g)	ν(pyr breath) i.ph.
1018							1016		Phenyl
1028	1029	1028	1027	1028	1028	1028	1028	ν_{15} (A_g)	ν(pyr breath) o.o.ph.
1214	1220	1207	1232	1214	1213	1213	1212		Phenyl
1260	1263	1263	1273	1261	1262	1261	1329	ν_1 (A_g)	ν(C_m–C_{ph}) sym
1397	1396	1396	1396	1397	1397	1396	1397	ν_4 (A_g)	ν(pyr/2) sym
1420	1419	1420	1419	1420	1420	1420	1420	ν_{29} (B_{1g})	ν(pyr/4) sym
1490	1489	1490	1488	1490	1491	1490	1494	ν_3 (A_g)	ν(C_α–C_m) i.ph.
1500	1497	1498	1496	1497	1497	1497	1500	ν_{28} (B_{1g})	ν(C_α–C_m) o.o.ph.
1542	1562	1563	1571	1559	1552	1538			Phenyl
1557	1554	1554	1553	1559	1559	1559	1557	ν_{11} (A_g)	ν(C_β–C_β) i.ph.
1597	1596	1596	1592	1596	1592	1596	1597	ν_{10} (A_g)	ν(C_α–C_m) asym
1610	1609	1608	1606	1610	1611	1611	1609	ν_2 (A_g)	ν(C_β–C_β) sym
1659	1670	1670	1671	1664	1662	1650	1651		Phenyl

* Symmetry species for H_2TPP (D_{2h} group).
** Abbreviations: i.ph. = in-phase, o.o.ph. = out-of-phase.

Table 2
Band positions and assignment of calculated infrared bands of **FB1-8**.

Band positions (cm^{-1})								Mode number	Assignment
FB1	**FB2**	**FB3**	**FB4**	**FB5**	**FB6**	**FB7**	**FB8**		
383	319	335	332	312	372	298	385	ν_{50b} (B_{3u})*	ν(pyr trans)
385	322	337	338	313	380	301	386	ν_{50a} (B_{2u})	ν(pyr trans)
425	393	393	372	350	389	365	402	ν_{49b} (B_{3u})	ν(pyr rot)
433	403	408	387	365	399	380	421	ν_{49a} (B_{2u})	ν(pyr rot)
673	600	608	600	708	781	718	775		Phenyl
716	723	720		752		832			Phenyl
			741	716	724	707	879		Phenyl
825	826	826	827	826	826	826	825	γ_{17} (B_{1u})	$\delta(C_\beta–H)/\delta(N–H)$ sym
830	862						923		Phenyl
	814	857				888			Phenyl
1009	1009	1009	1008	1009	1009	1009	1010	ν_{47a}, ν_{47b} (B_{2u}, B_{3u})	ν(pyr breath) asym
1018	1009	1009	1007	1003			1022		Phenyl
1024	1023	1022	1019	1023	1023	1023	1016	ν_{17} (B_{2u})	$\delta(C_\beta–H)$ sym
1109	1045	1032	1090	1046	1143	1132			Phenyl
1214	1220	1210	1230	1214	1231	1326			Phenyl
1386	1386	1377	1385	1349	1341	1357		ν_{39b} (B_{3u})	$\nu(C_\alpha–C_m)$ sym + Phenyl
1443	1442	1443	1442	1442	1442	1441	1443	ν_{39a} (B_{2u})	$\nu(C_\alpha–C_m)$ sym
1518	1516	1516	1509	1518	1519	1519	1518	ν_{38a} (B_{2u})	$\nu(C_\beta–C_\beta)$
1526	1526	1526	1524	1526	1526	1526	1528	ν_{38b} (B_{3u})	$\nu(C_\beta–C_\beta)$
1613	1611	1612	1612	1616	1614	1615	1613	ν_{37b} (B_{3u})	$\nu(C_\alpha–C_m)$ asym

* Symmetry species for H_2TPP (D_{2h} group).

3.2.1.3. ν_8 and ν_{18} modes. These two weak modes involve in-phase (ν_8) and out-of-phase (ν_{18}) symmetric porphyrin ring breathing motions, driven by the in-plane translation of the four pyrrole rings. ν_8 expresses mass-correlated bathochromic shift when para substituents are present on the phenyl rings (**FB2-7**). The lightest substituent, methyl group as in **FB2**, causes the calculated ν_8 breathing frequency of H_2TPP to shift from 339 to 334 cm^{-1}, while the heaviest substituent, methyl carboxyl group as in **FB5**, reduces the frequency further to 321 cm^{-1}. However, this effect is absent for **FB8**. This cancellation of mass effect could be explained by the coupling of ring breathing motion with the scissoring motion of the four pairs of meta-methyl groups perpendicular to the porphyrin ring, which is also a part of ν_8 mode for this particular molecule. For the out-of-phase ν_{18} mode, the substituents on phenyl rings do not change the vibration significantly as the breathing frequencies of substituted H_2TPP vary in a small range of 169–172 cm^{-1}.

3.2.2. Infrared spectra

In a similar manner to the Raman spectra discussion, the infrared counter part of this work started from the discussion on the substituent effects on the central porphine moiety of the H_2TPP molecule. Noticeable changes in infrared bands are discussed as following.

3.2.2.1. ν_{50} modes. This pair of modes represent the in-plane translations of pyrrole rings in two axes, separately numbered as ν_{50a} and ν_{50b} for B_{2u} and B_{3u} modes respectively. The infrared absorptions of these dual modes appear adjacently at 383 and 385 cm^{-1} for ν_{50b} and ν_{50a} respectively. The effect from para substituents tends to downshift the absorption frequencies especially for **FB7** of which the absorption bands are moved down to 298 and 301 cm^{-1} with a very pale intensity. The same effect is not observed in the meta-substituted analog, **FB8**, of which the band remains at 385 and 386 cm^{-1}.

3.2.2.2. ν_{49} modes. Similar to the neighboring ν_{50} modes, these modes represent the in-plane rotation of pyrrole rings in two axes. B_{2u} and B_{3u} modes are numbered as ν_{49a} and ν_{49b} respectively. However, unlike the pyrrolic translation modes, these sibling bands are more distant apart from each other. For H_2TPP, the calculation expects the bands at 403 and 425 cm^{-1} for ν_{49b} and ν_{49a} respectively. Introducing para substituents also induces a red shift similar to one in ν_{50}

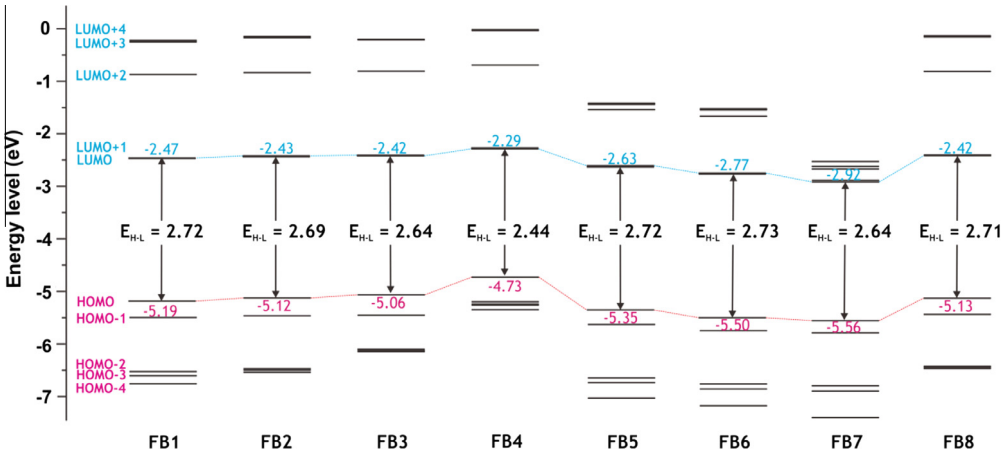

Fig. 3. Molecular orbital energy of **FB1-8** calculated by B3LYP/6-31G(d).

modes. The only exception is **FB7** of which the absorption bands rise to 483 and 490 cm^{-1}.

3.2.2.3. v_{39} modes. These modes represent symmetric C_α–C_m stretching modes with B_{2u} and B_{3u} characters. Neither does ν_{39a} mode of which the absorption bands stand still at 1442 ± 1 cm^{-1}. The substituent-dependence is found for ν_{39b} mode which vibrates concertedly with a symmetric phenyl hydrogen bending mode which will be discussed later on. The ν_{39b} band downshifts 30–50 cm^{-1} when electron withdrawing groups are present (**FB5**-7).

3.3. Electronic structures and spectra

The molecular orbital energy levels in the neighborhood of highest occupied molecular orbitals (HOMOs) and lowest unoccupied molecular orbitals (LUMOs) of H_2TPP and its derivatives are

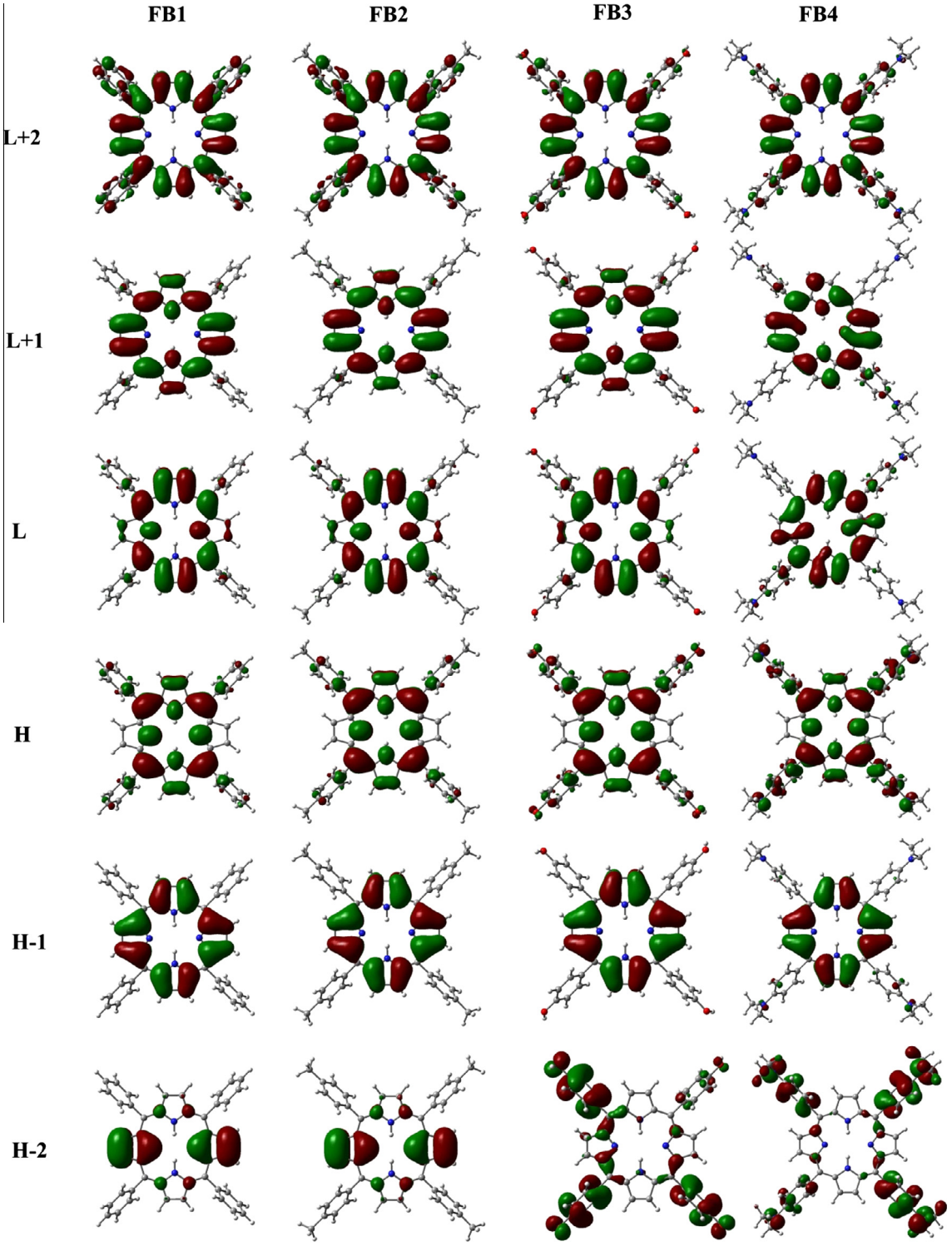

Fig. 4. Molecular orbitals relevant to the excitation of **FB1**-**4** calculated by B3LYP/6-31G(d).

visualized as a diagram in Fig. 3. From the diagram, derivatives with electron-donating substituents (**FB1**-4) are indifferent in energies of their HOMO and LUMO, notated by E_{HOMO} and E_{LUMO}, respectively, and thus indifferent in their HOMO–LUMO gap energies (E_{H-L}). There is an exception for the strongest donor in the series, dimethylamino group in **FB4**, of which HOMO and LUMO are significantly raised and E_{H-L} is reduced to 2.44 eV. However, the presence of electron donors on the phenyl rings

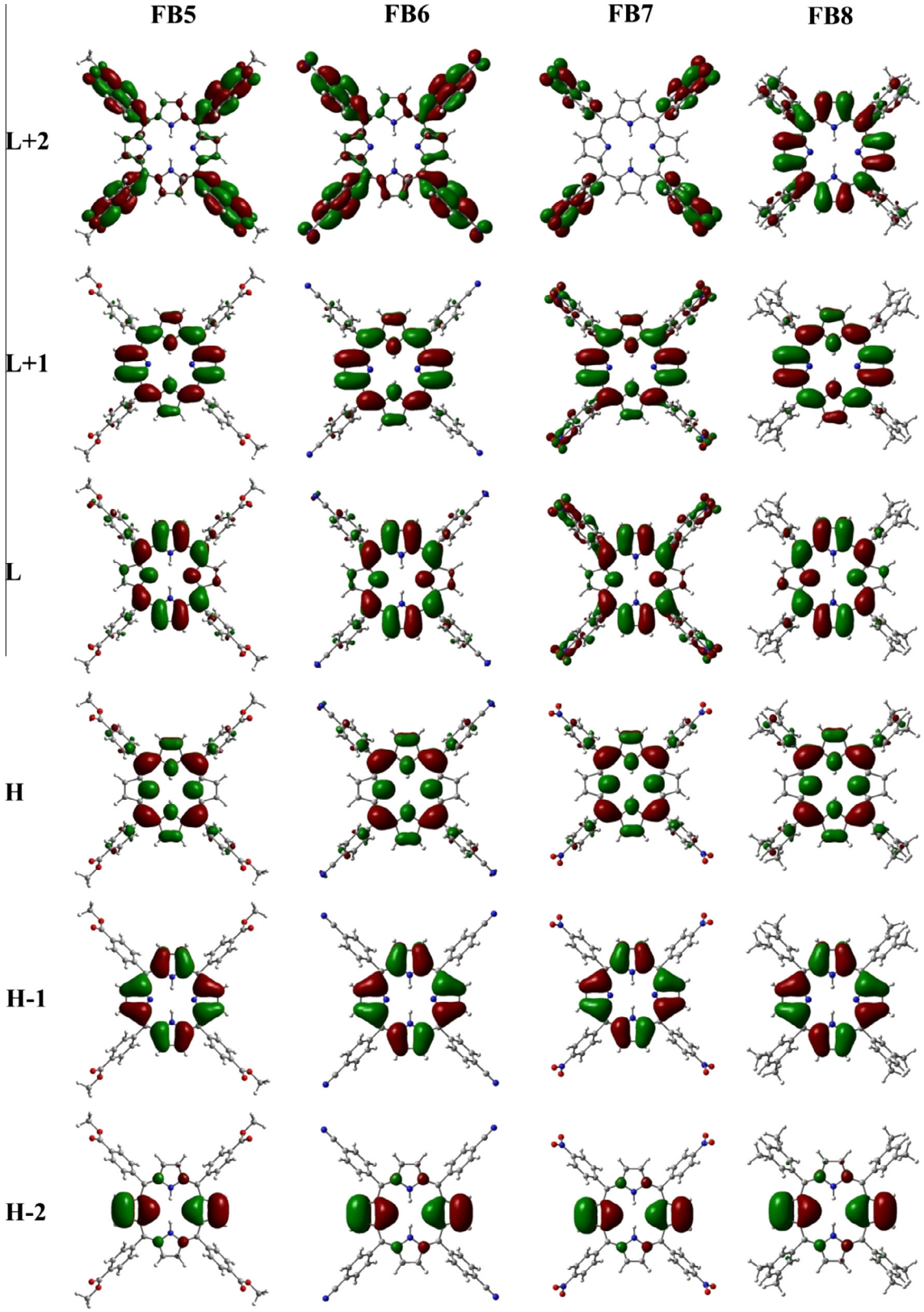

Fig. 5. Molecular orbitals relevant to the excitation of **FB5-8** calculated by B3LYP/6-31G(d).

affects more on the lower occupied orbital (e.g. HOMO-1, HOMO-2, HOMO-3, etc.) levels. For a strong electron donor like dimethylamino group, its effect squeezes the gap between HOMO-4 and HOMO (and all others in between) of **FB4** narrower than 1 eV. Especially, its HOMO-4, HOMO-3 and HOMO-2 are nearly degenerated. On the other hand, electron withdrawing groups (as in **FB5**-7) cause downshifts in E_{HOMO} and E_{LUMO}, but their E_{H-L} remain conserved compared to their parent, **FB1**. However, the energy levels of non-LUMO unoccupied orbitals are lowered closer to the LUMO levels on the effect of these substituents. In the case of a very strong electron withdrawer like nitro group in **FB7**, the first five unoccupied orbitals are stacked together within the interval of 0.5 eV. The meta-methyl-substituted **FB8** shows the orbital energy levels much similar to those of its methyl-substituted relative **FB2**, and has the gap energy close to those of **FB1**-3 and **FB5**-7.

Molecular orbitals visualization is also helpful with descriptive understanding on their excitation types. The molecular orbitals involved in the excitation are displayed in Figs. 4 and 5. The calculated orbital models reveal the π–π^* nature of the transition among HOMO, HOMO-1, LUMO and LUMO+1 for most of the studied derivatives. This is deduced from the localization of electrons on the π-orbitals on the porphine central rings. The exceptions are found for **FB4** and **FB7**, of which added substituents are very strong electron donor and withdrawer.

For **FB4**, phenyl π-orbitals have larger contribution to the HOMO compared those of the rest, while its LUMO and LUMO+1 contains no noticeable phenyl π-orbitals. This suggests that the HOMO → LUMO and HOMO → LUMO+1 excitations have mixed characters of π–π^* and charge-transfer transitions. The direction of the charge transfer is from the phenyl rings converging to the porphine center. Such charge redistribution is desirable in dye sensitizer with β-linked π-spacer as it resembles to one of ZnTMPPI in Ma et al.'s work [29].

A similar suggestion can also be applied to **FB7**, where the strong nitro substituents allow partial localization of π-electrons on outer phenyl rings for the LUMO and LUMO+1. This also leads to a prediction of mixed π–π^* and charge-transfer characters of the excitations toward these two orbitals. However, in this case, the charge transfer diverges from the central porphine π-system. This suggests the addition of meso-linked π-spacer **FB7** in the further dye development.

Further looking into the quantitative prediction of excitations, the excitation energies of relevant excitations are listed in Table 3. Transitions between HOMO, HOMO-1, LUMO and LUMO+1 are dominant in the absorption spectra for most H_2TPP derivatives (namely **FB1**-3, **FB5**-6 and **FB8**). This implies that these derivatives are well behaving to the Gouterman's four-orbital model [16]. Their predicted adsorption spectra (Fig. 6) are as well in a similar shape, intense B bands with maximum near 400 nm and tiny Q bands between 500 and 600 nm.

However, for **FB4** and **FB7**, their strong donating/withdrawing substituents have influence on the changing of preferred transitions and thus deviate from the Gouterman's model. The intense B band of **FB4** is mainly contributed by the transitions from HOMO-5 and HOMO-4 to LUMO+1, while one of **FB7** is the result of the

Table 3
Excitation wavelengths/energies (nm/eV), oscillator strengths and electronic configuration for **FB1-8** in CH_2Cl_2 calculated by TD-B3LYP/6-31G(d).

Molecule	Band	Excitation nm (eV)	Oscillator strength	One-electron transition (weight)	
FB1	B	399 (3.11)	1.7458	H-1 → L (64%)	H → L + 1 (35%)
		406 (3.06)	1.4161	H-1 → L + 1 (64%)	H → L (28%)
	Q	539 (2.30)	0.0555	H → L + 1 (65%)	H-1 → L (34%)
		575 (2.16)	0.0400	H → L (68%)	H-1 → L + 1 (32%)
FB2	B	402 (3.09)	1.7850	H-1 → L (66%)	H → L + 1 (32%)
		408 (3.04)	1.5112	H-1 → L + 1 (65%)	H → L (27%)
	Q	542 (2.29)	0.0762	H → L + 1 (67%)	H-1 → L (32%)
		578 (2.14)	0.0529	H → L (69%)	H-1 → L + 1 (30%)
FB3	B	409 (3.03)	1.5073	H-1 → L (63%)	H → L + 1 (26%)
		414 (2.99)	1.4275	H-1 → L + 1 (62%)	H → L (24%)
	Q	549 (2.26)	0.1026	H → L + 1 (71%)	H-1 → L (29%)
		585 (2.12)	0.0680	H → L (72%)	H-1 → L + 1 (28%)
FB4	B1	459 (2.70)	0.3446	H-4 → L + 1 (51%)	H-3 → L (44%)
	B2	386 (3.21)	1.4179	H-5 → L + 1 (46%)	H-4 → L (39%)
		396 (3.13)	1.0333	H-4 → L + 1 (45%)	H-5 → L (34%)
	Q	590 (2.10)	0.2890	H → L + 1 (85%)	H-4 → L (12%)
		620 (2.00)	0.1803	H → L (82%)	H-4 → L + 1 (15%)
FB5	B	406 (3.05)	1.8808	H-1 → L + 1 (55%)	H → L (29%)
		413 (3.00)	1.5934	H-1 → L (54%)	H → L + 1 (26%)
	Q	542 (2.29)	0.0775	H → L (58%)	H-1 → L + 1 (30%)
		576 (2.15)	0.0445	H → L + 1 (59%)	H-1 → L (29%)
FB6	B	406 (3.05)	1.8636	H-1 → L + 1 (60%)	H → L (33%)
		414 (3.00)	1.5572	H-1 → L (59%)	H → L + 1 (29%)
	Q	541 (2.29)	0.0705	H → L (64%)	H-1 → L + 1 (35%)
		575 (2.16)	0.0382	H → L + 1 (65%)	H-1 → L (33%)
FB7	B1	449 (2.76)	0.1110	H-1 → L + 5 (45%)	H-1 → L + 1 (40%)
	B2	390 (3.18)	1.5556	H-1 → L + 4 (35%)	H → L + 5 (26%)
				H-1 → L + 1 (22%)	H → L (13%)
		397 (3.12)	0.9894	H-1 → L + 5 (49%)	H → L + 4 (14%)
				H-1 → L (13%)	H-3 → L + 1 (11%)
	Q	556 (2.23)	0.1389	H → L (72%)	H-1 → L + 1 (25%)
		583 (2.12)	0.0581	H → L + 1 (63%)	H-1 → L (29%)
FB8	B	402 (3.09)	1.7435	H-1 → L (63%)	H → L + 1 (34%)
		408 (3.04)	1.4338	H-1 → L + 1 (64%)	H → L (28%)
	Q	540 (2.30)	0.0575	H → L + 1 (65%)	H-1 → L (35%)
		575 (2.15)	0.0423	H → L (68%)	H-1 → L + 1 (32%)

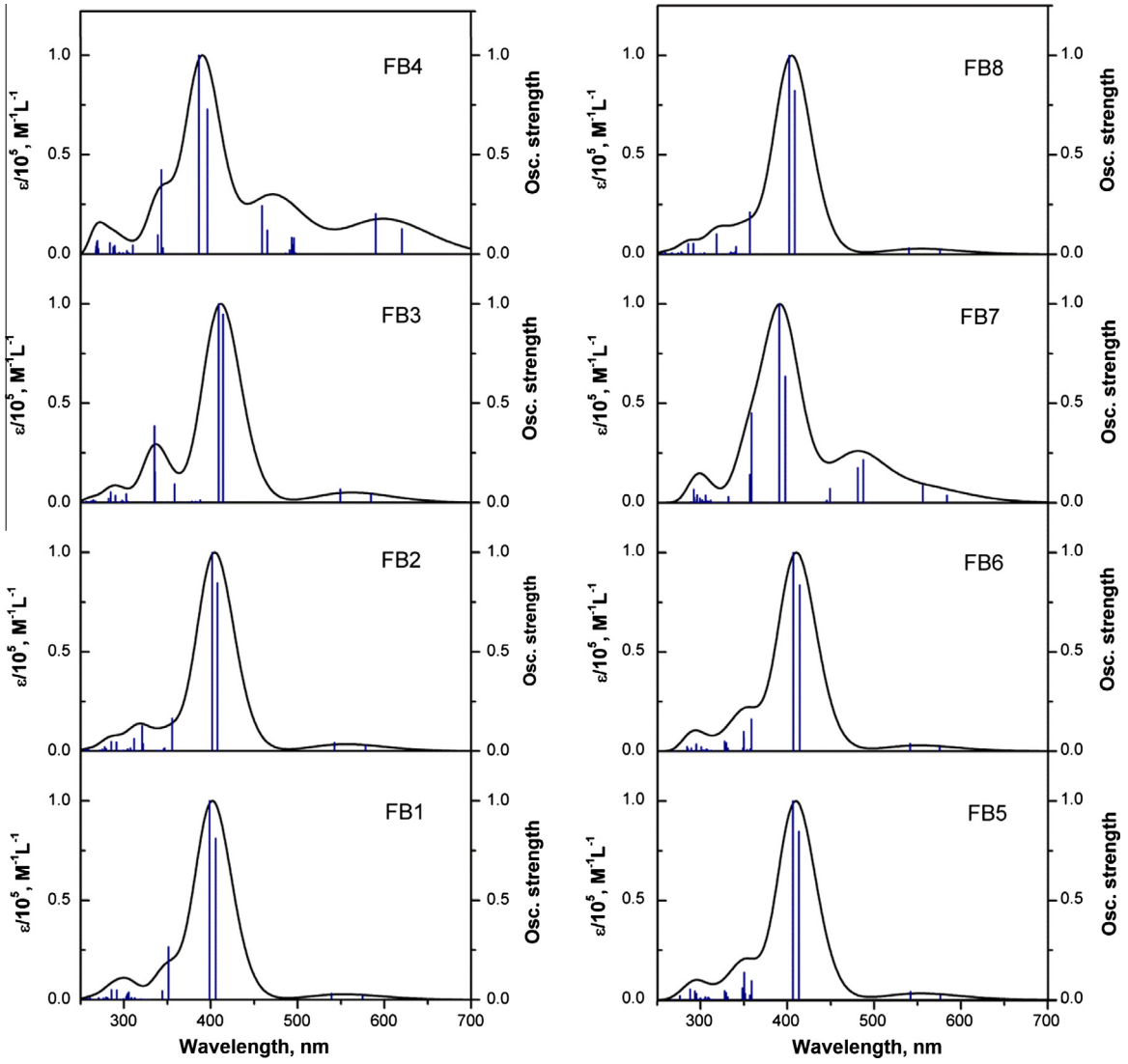

Fig. 6. Absorption spectra of **FB1-8** calculated by TD-B3LYP/6-31G(d) in CH_2Cl_2.

transitions from HOMO-1 to LUMO+4 and LUMO+5. These distant transitions lead to the expectation of blue shifts of their B bands, which is also noticeable on the plotted spectra. The blue shifts of both derivatives might disfavor the light-harvesting efficiency of the dye. However, the slight handicap is greatly compensated by their strong split B bands near 480 nm. This adds up more advantage of these two candidates over their counterparts.

The corresponding transitions of Q bands of **FB4** and **FB7** are also worth discussing for its involvement with charge-transfer excitation as previously discussed. The dominant Q band contributors of **FB4** and **FB7** are the transitions from HOMO to LUMO and LUMO+1, which are all expected to cause charge transfer. The charge transfer suggested for both compounds could also contribute to their stronger Q band intensities compared to other derivatives. Two Q bands at 590 and 620 nm are spotted with moderate intensities on **FB4** spectrum, which is far red-shifted and more intense than H_2TPP. Meanwhile, one Q band of **FB7** is gently red-shifted to 556 nm. However, the band is relatively pale and stands as a shoulder of its branched B band. This marks its inferiority to **FB4** as a dye-sensitizer candidate. Additionally, weights of first and second dominating B band transitions of **FB4** and **FB7** also appear to be more equally distributed than those of other derivatives. This can also be explained by the closer stacking of energy levels as illustrated in Fig. 3.

Electron-donators also express a noticeable trend of red-shifts in both Q bands and B bands with increasing electron-donating strength (from 575-nm Q band of **FB1** to 620-nm Q band of **FB4**). In contrary, this cannot be seen in the electron-withdrawing series. However, more results from additional substituents are needed to confirm this trend.

Considering all the spectroscopic predictions altogether, **FB4** gives obviously the broadest and most continuous absorption spectrum covering from ultraviolet to near-infrared. Combining this with its structural favor to electronic push–pull architecture, **FB4** makes the most promising candidates among the studied series and could serve as the template for a well-performing dye-sensitizer in DSSC.

4. Conclusions

The effects of common electron-donating and – withdrawing substituents introduced to the meso-phenyl rings of H_2TPP have been demonstrated in the calculated vibrational and electronic spectra. In the study of vibrational spectra, the trends regarding

the strength of electron-inducing substituents are mostly unclear, and mainly found on the phenyl rings.

However, the trends are relatively clearer in the electronic spectra as their molecular orbitals are more directly involved with the degrees of electron-inducing effects of the substituents. Electron-donating and -withdrawing substituents result in the blue shifts and the splits of Soret or B bands of H_2TPP. The blue shifts can be explained by the changes in the energy levels of non-HOMO/non-LUMO molecular orbitals, which allow electronics excitations from distant orbitals such as HOMO−5 or LUMO+5. In addition, H_2TPP also improves in its Q band absorbance as dimethylamino and nitro substituents are introduced to the phenyl moieties due to the increase of charge transfer character of the electronic transition, according to the molecular orbital inspection. However, the introduction of dimethylamino groups on phenyl rings has a potential to improve the Q band intensity by promoting the mobilization of excited electrons from the substituents to the porphine core, while the introduction of nitro groups does not. These findings can be helpful in the design and fine-adjustment of dye-sensitizer in solar cells.

Acknowledgments

The authors wish to thank Chiang Mai University and the National Research Council of Thailand for financial support and the Ministry of Energy for a grant to purchase computer hardware. The computer facility at the Nanoscale Simulation Laboratory in the National Nanotechnology Center (NANOTEC), Pathumthani and at the Department of Chemistry, Faculty of Science, Chiang Mai University, and Chiang Mai, Thailand are also acknowledged.

Appendix A. Supplementary material

Supplementary data associated with this article can be found, in the online version, at http://dx.doi.org/10.1016/j.comptc.2015.03.009.

References

[1] J.-H. Chou, M.E. Kosal, H.S. Nalwa, N.A. Rakow, K.S. Suslick, Applications of porphyrins and metalloporphyrins to materials chemistry, in: K.M. Kadish, K.M. Smith, R. Guilard (Eds.), The Porphyrin Handbook, Academic Press, 2000, p. 53.
[2] S. Gokulnath, T. Chandrashekar, Expanded porphyrins as third order non-linear optical materials: Some structure-function correlations, J. Chem. Sci. 120 (2008) 137–142.
[3] E.D. Sternberg, D. Dolphin, C. Brückner, Porphyrin-based photosensitizers for use in photodynamic therapy, Tetrahedron 54 (1998) 4151–4202.
[4] R. Wormald, J.R. Evans, L.L. Smeeth, K.S. Henshaw, Photodynamic therapy for neovascular age-related macular degeneration, Cochrane Database Syst. Rev. (2007).
[5] O. Finikova, A. Galkin, V. Rozhkov, M. Cordero, C. Hägerhäll, S. Vinogradov, Porphyrin and tetrabenzoporphyrin dendrimers: tunable membrane-impermeable fluorescent pH nanosensors, J. Am. Chem. Soc. 125 (2003) 4882–4893.
[6] L.B. Josefsen, J.W. Aylott, A. Beeby, P. Warburton, J.P. Boyle, C. Peers, R.W. Boyle, Porphyrin-nanosensor conjugates. New tools for the measurement of intracellular response to reactive oxygen species, Photochem. Photobiol. Sci. 9 (2010) 801–811.
[7] T. Bessho, S.M. Zakeeruddin, C.-Y. Yeh, E.W.-G. Diau, M. Grätzel, Highly efficient mesoscopic dye-sensitized solar cells based on donor–acceptor-substituted porphyrins, Angew. Chem. Int. Ed. 49 (2010) 6646–6649.
[8] W.M. Campbell, K.W. Jolley, P. Wagner, K. Wagner, P.J. Walsh, K.C. Gordon, L. Schmidt-Mende, M.K. Nazeeruddin, Q. Wang, M. Grätzel, D.L. Officer, Highly efficient porphyrin sensitizers for dye-sensitized solar cells, J. Phys. Chem. C 111 (2007) 11760–11762.
[9] S. Cherian, C.C. Wamser, Adsorption and photoactivity of tetra(4-carboxyphenyl)porphyrin (TCPP) on nanoparticulate TiO_2, J. Phys. Chem. B 104 (2000) 3624–3629.
[10] L.-L. Li, E.W.-G. Diau, Porphyrin-sensitized solar cells, Chem. Soc. Rev. 42 (2013) 291–304.
[11] M.K. Nazeeruddin, R. Humphry-Baker, D.L. Officer, W.M. Campbell, A.K. Burrell, M. Grätzel, Application of metalloporphyrins in nanocrystalline dye-sensitized solar cells for conversion of sunlight into electricity, Langmuir 20 (2004) 6514–6517.
[12] J.K. Park, H.R. Lee, J. Chen, H. Shinokubo, A. Osuka, D. Kim, Photoelectrochemical properties of doubly β-functionalized porphyrin sensitizers for dye-sensitized nanocrystalline-TiO_2 solar cells, J. Phys. Chem. C 112 (2008) 16691–16699.
[13] Q. Wang, W.M. Campbell, E.E. Bonfantani, K.W. Jolley, D.L. Officer, P.J. Walsh, K. Gordon, R. Humphry-Baker, M.K. Nazeeruddin, M. Grätzel, Efficient light harvesting by using green Zn–Porphyrin-sensitized nanocrystalline TiO_2 films, J. Phys. Chem. B 109 (2005) 15397–15409.
[14] A. Yella, H.-W. Lee, H.N. Tsao, C. Yi, A.K. Chandiran, M.K. Nazeeruddin, E.W.-G. Diau, C.-Y. Yeh, S.M. Zakeeruddin, M. Grätzel, Porphyrin-sensitized solar cells with cobalt (II/III)–based redox electrolyte exceed 12 percent efficiency, Science 334 (2011) 629–634.
[15] B. O'Regan, M. Gratzel, A low-cost, high-efficiency solar cell based on dye-sensitized colloidal TiO_2 films, Nature 353 (1991) 737–740.
[16] S. Mathew, A. Yella, P. Gao, R. Humphry-Baker, F.E. CurchodBasile, N. Ashari-Astani, I. Tavernelli, U. Rothlisberger, K. NazeeruddinMd, M. Grätzel, Dye-sensitized solar cells with 13% efficiency achieved through the molecular engineering of porphyrin sensitizers, Nat. Chem. 6 (2014) 242–247.
[17] M. Gouterman, G.H. Wagnière, L.C. Snyder, Spectra of porphyrins: Part II. Four orbital model, J. Mol. Spectrosc. 11 (1963) 108–127.
[18] L. Cai, T. Moehl, S.-J. Moon, J.-D. Decoppet, R. Humphry-Baker, Z. Xue, L. Bin, S.M. Zakeeruddin, M. Grätzel, 4,9-Dihydro-4,4,9,9-tetrahexyl-s-indaceno [1,2-b:5,6-b′]dithiophene as a π-spacer of donor−π–acceptor dye and its photovoltaic performance with liquid and solid-state dye-sensitized solar cells, Org. Lett. 16 (2013) 106–109.
[19] S. Chaurasia, C.-Y. Hsu, H.-H. Chou, J.T. Lin, Synthesis, optical and electrochemical properties of pyridal[2,1,3]thiadiazole based organic dyes for dye sensitized solar cells, Org. Electron. 15 (2014) 378–390.
[20] S. Namuangruk, K. Sirithip, R. Rattanatwan, T. Keawin, N. Kungwan, T. Sudyodsuk, V. Promarak, Y. Surakhot, S. Jungsuttiwong, Theoretical investigation of the charge-transfer properties in different meso-linked zinc porphyrins for highly efficient dye-sensitized solar cells, Dalton Trans. 43 (2014) 9166–9176.
[21] M.-J. Lee, M. Balanay, D. Kim, Molecular design of distorted push–pull porphyrins for dye-sensitized solar cells, Theor. Chem. Acc. 131 (2012) 1–12.
[22] C.-W. Lee, H.-P. Lu, C.-M. Lan, Y.-L. Huang, Y.-R. Liang, W.-N. Yen, Y.-C. Liu, Y.-S. Lin, E.W.-G. Diau, C.-Y. Yeh, Novel zinc porphyrin sensitizers for dye-sensitized solar cells: synthesis and spectral, electrochemical, and photovoltaic properties, Chem. – A Europ. J. 15 (2009) 1403–1412.
[23] C.-P. Hsieh, H.-P. Lu, C.-L. Chiu, C.-W. Lee, S.-H. Chuang, C.-L. Mai, W.-N. Yen, S.-J. Hsu, E.W.-G. Diau, C.-Y. Yeh, Synthesis and characterization of porphyrin sensitizers with various electron-donating substituents for highly efficient dye-sensitized solar cells, J. Mater. Chem. 20 (2010) 1127–1134.
[24] H.-P. Lu, C.-Y. Tsai, W.-N. Yen, C.-P. Hsieh, C.-W. Lee, C.-Y. Yeh, E.W.-G. Diau, Control of dye aggregation and electron injection for highly efficient porphyrin sensitizers adsorbed on semiconductor films with varying ratios of coadsorbate, J. Phys. Chem. C 113 (2009) 20990–20997.
[25] S.-L. Wu, H.-P. Lu, H.-T. Yu, S.-H. Chuang, C.-L. Chiu, C.-W. Lee, E.W.-G. Diau, C.-Y. Yeh, Design and characterization of porphyrin sensitizers with a push–pull framework for highly efficient dye-sensitized solar cells, Energy Environ. Sci. 3 (2010) 949–955.
[26] A.D. Becke, Density-functional thermochemistry. III. The role of exact exchange, J. Chem. Phys. 98 (1993) 5648–5652.
[27] N.N. Matsuzawa, A. Ishitani, D.A. Dixon, T. Uda, Time-dependent density functional theory calculations of photoabsorption spectra in the vacuum ultraviolet region, J. Phys. Chem. A 105 (2001) 4953–4962.
[28] M.P. Balanay, K.H. Kim, S.H. Lee, D.H. Kim, Tuning the photovoltaic parameters of β-substituted porphyrin analogues: An experimental and theoretical approach, J. Photochem. Photobiol., A 248 (2012) 63–72.
[29] R. Ma, P. Guo, H. Cui, X. Zhang, M.K. Nazeeruddin, M. Grätzel, Substituent effect on the meso-substituted porphyrins: theoretical screening of sensitizer candidates for dye-sensitized solar cells, J. Phys. Chem. A 113 (2009) 10119–10124.
[30] P.J. Walsh, K.C. Gordon, D.L. Officer, W.M. Campbell, A DFT study of the optical properties of substituted Zn(II)TPP complexes, J. Mol. Struct. (Thoechem) 759 (2006) 17–24.
[31] C. Lee, W. Yang, R.G. Parr, Development of the Colle-Salvetti correlation-energy formula into a functional of the electron density, Phys. Rev. B 37 (1988) 785–789.
[32] B. Miehlich, A. Savin, H. Stoll, H. Preuss, Results obtained with the correlation energy density functionals of becke and Lee, Yang and Parr, Chem. Phys. Lett. 157 (1989) 200–206.
[33] M. Cossi, V. Barone, Time-dependent density functional theory for molecules in liquid solutions, J. Chem. Phys. 115 (2001) 4708–4717.
[34] P. Ordon, A. Tachibana, Investigation of the role of the C-PCM solvent effect in reactivity indices, J. Chem. Sci. 117 (2005) 583–589.
[35] N.M. O'Boyle, A.L. Tenderholt, K.M. Langner, Cclib: A library for package-independent computational chemistry algorithms, J. Comput. Chem. 29 (2008) 839–845.
[36] M.J. Frisch, G.W. Trucks, H.B. Schlegel, G.E. Scuseria, M.A. Robb, J.R. Cheeseman, G. Scalmani, V. Barone, B. Mennucci, G.A. Petersson, H. Nakatsuji, M. Caricato, X. Li, H.P. Hratchian, A.F. Izmaylov, J. Bloino, G. Zheng, J.L. Sonnenberg, M. Hada, M. Ehara, K. Toyota, R. Fukuda, J. Hasegawa, M. Ishida, T. Nakajima, Y. Honda, O. Kitao, H. Nakai, T. Vreven, J.A. Montgomery Jr., J.E. Peralta, F. Ogliaro,

M.J. Bearpark, J. Heyd, E.N. Brothers, K.N. Kudin, V.N. Staroverov, R. Kobayashi, J. Normand, K. Raghavachari, A.P. Rendell, J.C. Burant, S.S. Iyengar, J. Tomasi, M. Cossi, N. Rega, N.J. Millam, M. Klene, J.E. Knox, J.B. Cross, V. Bakken, C. Adamo, J. Jaramillo, R. Gomperts, R.E. Stratmann, O. Yazyev, A.J. Austin, R. Cammi, C. Pomelli, J.W. Ochterski, R.L. Martin, K. Morokuma, V.G. Zakrzewski, G.A. Voth, P. Salvador, J.J. Dannenberg, S. Dapprich, A.D. Daniels, Ö. Farkas, J.B. Foresman, J.V. Ortiz, J. Cioslowski, D.J. Fox, Gaussian 09, Gaussian Inc, Wallingford, CT, USA, 2009.

[37] A.-R. Allouche, Gabedit-A graphical user interface for computational chemistry softwares, J. Comput. Chem. 32 (2011) 174–182.

[38] X.Y. Li, M.Z. Zgierski, Porphine force field: in-plane normal modes of free-base porphine; comparison with metalloporphines and structural implications, J. Phys. Chem. 95 (1991) 4268–4287.

[39] Y.-H. Zhang, W. Zhao, P. Jiang, L.-J. Zhang, T. Zhang, J. Wang, Structural parameters and vibrational spectra of a series of zinc meso-phenylporphyrins: A DFT and experimental study, Spectrochim. Acta Part A Mol. Biomol. Spectrosc. 75 (2010) 880–890.

[40] G.P. Moss, Nomenclature of tetrapyrroles. Recommendations, IUPAC-IUB Joint Commission on Biochemical Nomenclature (JCBN), Eur. J. Biochem. 178 (1988) (1986) 277–328.